INORGANIC CHEMISTRY FRONTIERS

RESEARCH ARTICLE

View Article Online
View Journal

Cite this: DOI: 10.1039/d5qi02451j

Multicolor and reversible stimuli-responsive luminescence of dumbbell-shaped Zn(II) complexes with extended triphenylamine-attached ethynylpyridine terminals

Yuta Takeuchi,[a] Minoru Yamada,[b] Itaru Tsuchiya,[c] Yoshiki Ozawa,[c] Masaaki Abe[c] and Akiko Hori *[a,b]

Dumbbell-shaped Zn(II) paddlewheel dimers bearing π-extended triphenylamine–ethynylpyridine ligands were synthesized to investigate how fluorination and axial π-extension influence structural flexibility and luminescence responsiveness. Single-crystal X-ray diffraction revealed that the benzoate and pentafluorobenzoate derivatives retain the Zn_2(μ-carboxylate)$_4$ core but differ in carboxylate planarity, intermolecular contacts, and overall molecular distortion. These subtle structural variations strongly affect their excited-state landscapes. The fluorinated complex exhibits an additional intramolecular charge-transfer absorption band and enhanced electronic anisotropy, leading to pronounced changes in the solid-state emission. Both complexes display reversible mechanochromic luminescence associated with partial amorphization and recrystallization, while the fluorinated derivative undergoes a larger red shift and higher quantum yield after grinding. High-pressure photoluminescence measurements on single crystals revealed continuous and nearly reversible emission shifts. The fluorinated complex shows a substantial 83 nm shift (ΔE = 0.36 eV) and a full multicolor progression from green to orange-red up to 3.6 GPa, whereas the non-fluorinated analogue displays only modest changes. These behaviors demonstrate that fluorination increases structural flexibility and enhances the pressure adaptability of the Zn_2 core. The results establish a design strategy in which a d^{10} metal scaffold is combined with electronically tunable π-extended axial ligands to achieve multicolor, reversible, and stimuli-responsive luminescence in simple molecular assemblies.

Received 3rd December 2025,
Accepted 18th January 2026

DOI: 10.1039/d5qi02451j

rsc.li/frontiers-inorganic

Introduction

Paddlewheel-type dinuclear Zn(II) complexes have long been employed as structurally well-defined molecular models that connect two metal centers through four bridging carboxylate ligands.[1–3] They have served as key building blocks in metal–organic frameworks and supramolecular assemblies,[4–9] and as model systems for investigating metal–metal interactions and photophysical modulation.[10,11] Among them, Zn(II) paddlewheel dimers, Zn_2(μ-carboxylate)$_4$, are particularly attractive because their d^{10} configuration prevents metal-centered emission, so the luminescence arises entirely from coordinated π-conjugated ligands.[12–14] Subtle changes in Zn(II)···Zn(II) separation or carboxylate geometry have been correlated with solid-state luminescence shifts, including in silica-bridged or hybrid matrices,[15] leading to mechanochromic or vapochromic responses under external stimuli such as mechanical stress or solvent vapor exposure.[16–18] Although Zn(II) complexes are widely used across coordination chemistry, their photophysical behavior is fundamentally constrained by the d^{10} configuration, which eliminates low-energy d–d transitions and renders the metal center essentially colorless.[19,20] As a result, visible absorption and emission in Zn(II) compounds originate almost exclusively from ligand-centered π–π* or n–π* transitions, with negligible contribution from Zn-based orbitals. This characteristic places Zn(II) paddlewheel dimers in a distinctive position among d-block systems: the metal–carboxylate framework provides structural rigidity and low toxicity while delegating electronic tunability entirely to the coordinated chromophoric ligands.[21,22] Despite this advantage,

[a]Graduate School of Engineering and Science, Shibaura Institute of Technology, Fukasaku 307, Minuma-ku, Saitama 337-8570, Japan.
E-mail: ahori@shibaura-it.ac.jp
[b]Undergraduate School of Engineering, Shibaura Institute of Technology, Fukasaku 307, Minuma-ku, Saitama 337-8570, Japan
[c]Graduate School of Science, University of Hyogo, 3-2-1 Kouto, Kamigori, Ako, Hyogo 678-1297, Japan

only a limited number of studies have exploited such d^{10} architectures to engineer long-range electronic communication or stimulus-responsive luminescence using π-extended axial ligands.[23,24] Establishing design principles for color-tunable Zn(II) assemblies therefore remains an important challenge in developing safe, cost-effective, and electronically modular luminescent materials.

Nevertheless, most reported Zn(II) paddlewheel dimers rely on simple carboxylate or pyridine ligands (*e.g.*, $[Zn_2(\mathbf{1})_4Py_2]$ in Fig. 1),[25,26] and examples that incorporate extended π-systems for detailed photophysical studies remain limited.[1–9,27–30] To address these points, we designed a new class of dumbbell-shaped Zn(II) paddlewheel dimers, $[Zn_2(\mathbf{n})_4L_2]$ (**n** = **1**, **2**), axially coordinated by π-extended triphenylamine-ethynyl-pyridine ligands (L). The Zn_2(μ-carboxylate)$_4$ core acts as a flexible coordination unit, while the conjugated termini provide long-range electronic communication over approximately three nanometers. Incorporation of fluorinated carboxylate bridges increases structural flexibility and electronic anisotropy, making the emission more responsive to mechanical stress, temperature, and pressure. This fluorination-induced adaptability enables gradual and reversible multicolor modulation across the visible range, consistent with progressive changes in π–π and π-hole···π interactions[31,32] within the crystal lattice. Herein, we describe the synthesis, crystal structures, and photophysical properties of these triphenylamine (TPA)-capped Zn(II) paddlewheel dimers, focusing on reversible mechanochromic and pressure-dependent luminescence.[16–18] The present study shows that combining a d^{10} metal core with π-extended, electronically tunable ligands provides a simple molecular strategy for developing adaptive luminescent materials that respond to external stimuli. The synthesized complexes display well-defined paddlewheel structures with extended axial ligands, enabling systematic evaluation of how fluorination and external stimuli influence their optical behavior. Both the benzoate (**1**) and pentafluorobenzoate (**2**) derivatives crystallize as pale-yellow solids but show distinct luminescence colors in the solid state: bluish-green for $[Zn_2(\mathbf{1})_4L_2]$ and yellow for $[Zn_2(\mathbf{2})_4L_2]$. Upon gentle grinding, both emissions shift to longer wavelengths and are fully restored after exposure to solvent vapor. These observations highlight the mechanical adaptability of the Zn_2(μ-carboxylate)$_4$ framework combined with the π-extended TPA–CC–Py ligands.

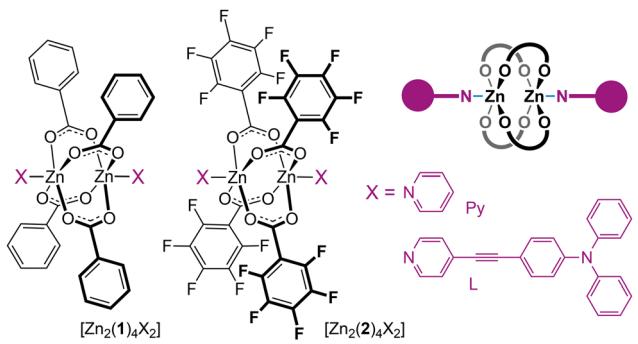

Fig. 1 Molecular structures of $[Zn_2(\mathbf{n})_4X_2]$ (**n** = **1** and **2**, X = Py and L); L = *N*,*N*-diphenyl-4-(pyridin-4-ylethynyl)aniline.

Results and discussion

Synthetic procedures and crystallographic studies

The π-extended ligand (L) was synthesized *via* a Sonogashira coupling between 4-bromopyridine and 4-ethynyl-*N*,*N*-diphenylaniline (Fig. S1).[33] The corresponding Zn(II) complexes $[Zn_2(\mathbf{n})_4L_2]$ (**n** = **1** and **2**) were prepared by reacting $Zn(OAc)_2{\cdot}2H_2O$ with benzoic acid (**H1**) or pentafluorobenzoic acid (**H2**) as bridging ligands in the presence of L as an axial donor in methanol. For comparison, the pyridine-capped analogues $[Zn_2(\mathbf{n})_4Py_2]$ were obtained under identical conditions.[26] The products were isolated as colorless solids for $[Zn_2(\mathbf{n})_4Py_2]$ and orange solids for $[Zn_2(\mathbf{n})_4L_2]$. The ^{1}H NMR spectra confirmed the formation of single-component dinuclear species (Fig. S2–5). Single crystals suitable for X-ray diffraction were obtained by slow evaporation of chloroform solutions, affording block-shaped crystals of $[Zn_2(\mathbf{n})_4Py_2]$ and $[Zn_2(\mathbf{n})_4L_2]$ (**n** = **1** and **2**) (Table S1, Fig. S6–S11).

Single-crystal analyses revealed that all complexes possess the typical paddlewheel-type dinuclear Zn(II) core bridged by four syn–syn carboxylate ligands (Fig. 2).† Each Zn(II) center adopts a distorted square-pyramidal geometry, coordinated by four oxygen atoms from the carboxylate ligands in the equatorial plane and one nitrogen atom from the axial ligand at the apical position. As summarized in Table 1, the Zn···Zn separations fall within the range commonly observed for Zn(II) paddlewheel dimers. The fluorinated complexes $[Zn_2(\mathbf{2})_4X_2]$ (X = Py and L) exhibit slightly longer Zn···Zn and shorter Zn–N distances, consistent with the electron-withdrawing fluorine atoms attached to the bridging ligands, which reduces the electron-donating ability toward the Zn(II) centers. In addition, the steric hindrance of the fluorine substituents (with a larger twist angle between the C_6F_5 and COO planes) appears to enhance the structural flexibility of the molecules.

In the L-containing complexes, each pyridyl group of L coordinates axially to the Zn_2 core to form a dumbbell-shaped molecular rod in which the nitrogen atoms of the terminal triphenylamine units are separated by around 28 Å, while the terminal C···C distance extends to approximately 34 Å, providing sufficient molecular length and rigidity. In $[Zn_2(\mathbf{1})_4L_2]$, the ethynyl–pyridine spacer adopts an almost linear geometry

†Crystal data of $[Zn_2(\mathbf{2})_4Py_2]$: $C_{38}H_{10}F_{20}N_2O_8Zn_2$ (m.w. 1133.22), orthorhombic, *Pbca*, T = 100 K, a = 19.6600(13) Å, b = 8.3244(6) Å, c = 23.6741(17) Å, V = 3874.4(5) Å^3, Z = 4, R = 0.0368, wR = 0.0986, GOF = 1.101. $[Zn_2(\mathbf{1})_4L_2]$: $C_{78}H_{56}N_4O_8Zn_2$ (m.w. 1308.00), triclinic, $P\bar{1}$, T = 100 K, a = 10.0947(18) Å, b = 10.1964(18) Å, c = 17.021(4) Å, α = 106.708(7)°, β = 102.504(7)°, γ = 96.097(6)°, V = 1611.4(5) Å^3, Z = 1, R = 0.0549, wR = 0.1461, GOF = 0.995. $[Zn_2(\mathbf{2})_4L_2]$: $C_{82}H_{36}F_{20}N_4O_{10}Zn_2$ (m.w. 1747.89), triclinic, $P\bar{1}$, T = 100 K, a = 11.713(7) Å, b = 12.142(7) Å, c = 14.308(7) Å, α = 111.447(19)°, β = 91.149(19)°, γ = 99.759(18)°, V = 1859.2(18) Å^3, Z = 1, R = 0.0933, wR = 0.2727, GOF = 0.975; T = 293 K, a = 11.7959(5) Å, b = 12.2469(5) Å, c = 14.3407(4) Å, α = 110.859(3)°, β = 91.242(3)°, γ = 100.562(4)°, V = 1894.58(13) Å^3, Z = 1, R = 0.0387, wR = 0.1065, GOF = 1.065.

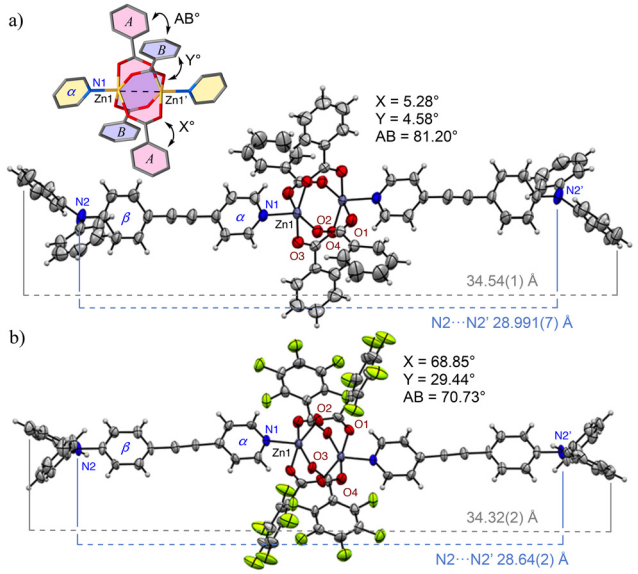

Fig. 2 Molecular structures with the selected numbering schemes of (a) $[Zn_2(\mathbf{1})_4L_2]$ (CCDC 2506029) and (b) $[Zn_2(\mathbf{2})_4L_2]$ (CCDC 2506030): ORTEP view with 50% thermal ellipsoids; color scheme: C, gray; N, blue; O, red; F, green; Zn, light blue.†

(Fig. 2a), and no significant intermolecular π···π interactions were observed. The detectable contacts were intermolecular CH···π interactions between ring-α and the terminal phenyl groups or between phenyl groups [C16–H16···C_g(Ph), C30–H30···C_g(Ph); C_g = centroid of the six-membered ring], and a pseudo-hydrogen bond between ring-α and an oxygen atom (C18–H18···O3). In contrast, the introduction of electron-withdrawing fluorine substituents decreases the planarity of the carboxylate bridges, giving a more flexible framework (Fig. 2b). The overall molecular shape displays a gentle wave-like distortion, and the intermolecular π-hole···π distance between adjacent molecules of C_6F_5 and C_6H_4(ring-β) groups is 3.826(6) Å (Fig. 3). Additional interactions include CH···π contacts between ring-α and the terminal phenyl group [C18–H18···C_g(Ph), C35–H35···C_g(α)], C–F···π interactions [C13–F9···C_g(β), C14–F10···C_g(β)], and a pseudo-hydrogen bond between ring-β and fluorine (C23–H23···F4). Hirshfeld surface (HS) analysis[34,35] supports these intermolecular interactions, as shown in Fig. S12–15. These subtle electronic and structural

Table 1 Selected intramolecular atom···atom distances (Å) for $[Zn_2(\mathbf{n})_4X_2]$ (**n** = **1** and **2**)

	$[Zn_2(\mathbf{1})_4Py_2]^a$	$[Zn_2(\mathbf{2})_4Py_2]$	$[Zn_2(\mathbf{1})_4L_2]$	$[Zn_2(\mathbf{2})_4L_2]$
Zn1···Zn1	2.958(3)	3.058(1)	2.945(8)	3.012(2)
Zn1···O1–4 (av.)	2.040	2.049	2.043	2.042
Zn1···N1	2.034(2)	2.016(3)	2.049(3)	2.017(9)
N(TPA)···N (TPA)	—	—	28.991(7)	28.64(2)
Longest C···C	13.69(4)	12.61(6)	34.54(1)^b	34.32(2)^b

^{a} Ref. 26; CCDC 610568. ^{b} C30···C30′ and C36···C36′ for $[Zn_2(\mathbf{1})_4X_2]$ and $[Zn_2(\mathbf{2})_4X_2]$, respectively.

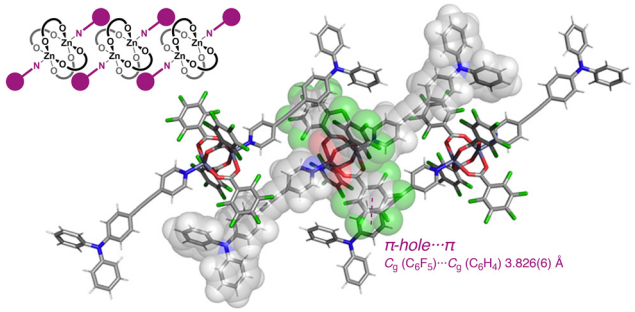

Fig. 3 Partial molecular packing of $[Zn_2(\mathbf{2})_4L_2]$.

variations are expected to play an important role in the luminescence behavior of the complexes. Such variations in carboxylate planarity and π-stacking geometry modulate the local electronic environment around the Zn_2 core, creating distinct excited-state landscapes that are highly sensitive to external perturbations.

Emission studies in solution and solid states

Both $[Zn_2(\mathbf{n})_4Py_2]$ complexes are colorless and show almost no emission in $CHCl_3$ solution (Table 2 and Fig. S16). In contrast, the dumbbell-shaped $[Zn_2(\mathbf{n})_4L_2]$ complexes form yellow solutions that exhibit intense blue luminescence under UV light. Their UV–Vis spectra in $CHCl_3$ show absorption maxima nearly identical to that of the free ligand L, indicating that the Zn_2(μ-carboxylate)$_4$ framework has little influence on the π-conjugated system. Thus, the two terminal TPA–CC–Py units behave as electronically independent chromophores. In the fluorinated complex $[Zn_2(\mathbf{2})_4L_2]$, an additional absorption band appears around 400 nm, which is attributed to an intramolecular charge-transfer (ICT) transition from the triphenylamine donor to the electron-deficient C_6F_5 group, as shown by DFT calculations (Fig. S17). The nearly identical spectral features among L and $[Zn_2(\mathbf{n})_4L_2]$ are consistent with only modest perturbation of the frontier orbitals by the paddlewheel core. The well-resolved ^{1}H NMR spectra in low-polarity halogenated

Table 2 Photophysical properties of $[Zn_2(\mathbf{n})_4X_2]$ (**n** = **1** and **2**); maximum absorption wavelength (λ_{abs}), emission wavelength (λ_{em}) with the excitation at λ_{ex} = 380 nm, and PL quantum yield (Φ_{PL})

		λ_{abs}/nm	λ_{em}/nm	Φ_{PL}
In $CHCl_3$ ^{a}	$[Zn_2(\mathbf{1})_4Py_2]$	264	Not detected	—
	$[Zn_2(\mathbf{2})_4Py_2]$	264	Not detected	—
	$[Zn_2(\mathbf{1})_4L_2]$	370	457	90
	$[Zn_2(\mathbf{2})_4L_2]$	373	459	86
	L only	370	456	78
Solid^b	$[Zn_2(\mathbf{1})_4Py_2]$	281	466	23
	$[Zn_2(\mathbf{2})_4Py_2]$	287	468	18
	$[Zn_2(\mathbf{1})_4L_2]$	392	487	17
	$[Zn_2(\mathbf{2})_4L_2]$	384	531	17
	L only	359	459	9

^{a} Other solvents were summarized in SI. ^{b} Microcrystalline samples were used.

solvents confirm that the dinuclear structure is retained in solution, lending support to this interpretation. These observations also suggest that the excited states remain largely confined to each TPA–CC–Py chromophore.

The emission spectra of L, $[Zn_2(\mathbf{1})_4L_2]$, and $[Zn_2(\mathbf{2})_4L_2]$ in solution show almost identical maxima at 456, 457, and 459 nm, respectively, suggesting that coordination does not significantly alter the excited-state energy levels (Fig. 4a and S18–S20). However, the photoluminescence quantum yields (Φ_{PL}) increase from 78% for L[33] to 90% for $[Zn_2(\mathbf{1})_4L_2]$ and 86% for $[Zn_2(\mathbf{2})_4L_2]$, indicating that Zn(II) coordination effectively suppresses nonradiative decay pathways. Solid-state luminescence was also investigated using microcrystalline samples. The colorless $[Zn_2(\mathbf{n})_4Py_2]$ complexes exhibit weak greenish-blue emission under UV irradiation (λ_{ex} = 380 nm), with maxima at 466 nm (Φ_{PL} = 23%) for $[Zn_2(\mathbf{1})_4Py_2]$ and 468 nm (Φ_{PL} = 18%) for $[Zn_2(\mathbf{2})_4Py_2]$ (Fig. 4b). The spectral similarity implies that the emission originates from the intrinsic Zn(II) paddlewheel framework rather than from the substituents or axial ligands. In contrast, $[Zn_2(\mathbf{1})_4L_2]$ emits bluish-white light, while $[Zn_2(\mathbf{2})_4L_2]$ shows yellow emission, with maxima at 487 nm (Φ_{PL} = 17%) and 531 nm (Φ_{PL} = 17%), respectively (Fig. 4c). The red shift observed upon fluorination suggests that the electron-withdrawing C_6F_5 groups modify the local packing environment, enhance π-conjugation, and stabilize the electronic structure along the paddlewheel's longitudinal axis. Since photoluminescence quantum yields are higher in dilute solution, where intermolecular interactions and self-absorption introduce additional nonradiative decay pathways, the reduced Φ_{PL} observed for the solid samples are therefore attributed to aggregation-related quenching effects rather than changes in the intrinsic emissive nature of the TPA–CC–Py chromophore.

In particular, the introduction of C_6F_5 groups increases the electronic anisotropy of the crystal lattice, strengthening π-hole···π interactions and generating a more polarizable environment in the solid state. These effects collectively promote stabilization of lower-energy excited states, leading to pronounced bathochromic shifts compared to non-fluorinated analogues. Encouraged by this bathochromic trend, we examined the temperature dependence of the single-crystal emissions (Fig. 4d).[36,37] For $[Zn_2(\mathbf{1})_4L_2]$, the emission profile remained almost unchanged, with the peak slightly shifting from 466 nm at 298 K to 463 nm at 78 K, while the intensity approximately doubled. This moderate enhancement is attributed to suppression of thermally activated nonradiative pathways in the rigid crystal lattice. In contrast, the fluorinated $[Zn_2(\mathbf{2})_4L_2]$ displayed a fourfold increase in intensity upon cooling, accompanied by a slight red shift from 502 nm (298 K) to 508 nm (78 K) and the emergence of an additional shoulder band around 475 nm. Such thermally induced spectral changes suggest a more flexible excited-state landscape and prompted further investigation of its external-field responsiveness.

Mechanochromic photoluminescence switching

When the crystalline samples were gently ground in a mortar, their emission colors changed markedly (Fig. 5a): from bluish-white to green for $[Zn_2(\mathbf{1})_4L_2]$ and from greenish-yellow to orange for $[Zn_2(\mathbf{2})_4L_2]$, accompanied by red shifts of 43 nm (Φ_{PL} = 15%) and 73 nm (Φ_{PL} = 36%), respectively (Fig. 5b).

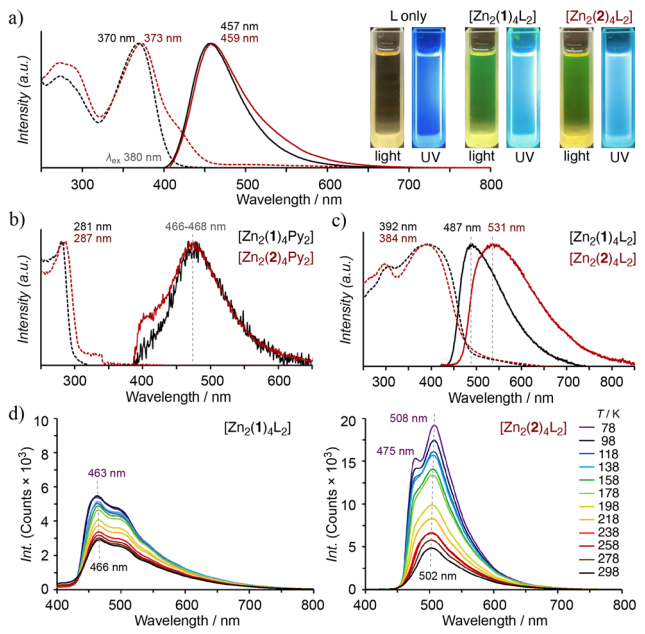

Fig. 4 Normalized UV-Vis and emission spectra of $[Zn_2(\mathbf{n})_4X_2]$: (a) $[Zn_2(\mathbf{n})_4L_2]$ in $CHCl_3$ solution with the corresponding appearances (0.1 mM); normalized UV-Vis and emission spectra of solid states for (b) $[Zn_2(\mathbf{n})_4Py_2]$ and (c) $[Zn_2(\mathbf{n})_4L_2]$; (d) the temperature-dependent emission (λ_{ex} = 380 nm) of $[Zn_2(\mathbf{n})_4L_2]$ at 78–298 K. Color scheme: (a–c) black, non-fluorinated complex; red, fluorinated complex; dashed line, absorption; solid line, emission spectra.

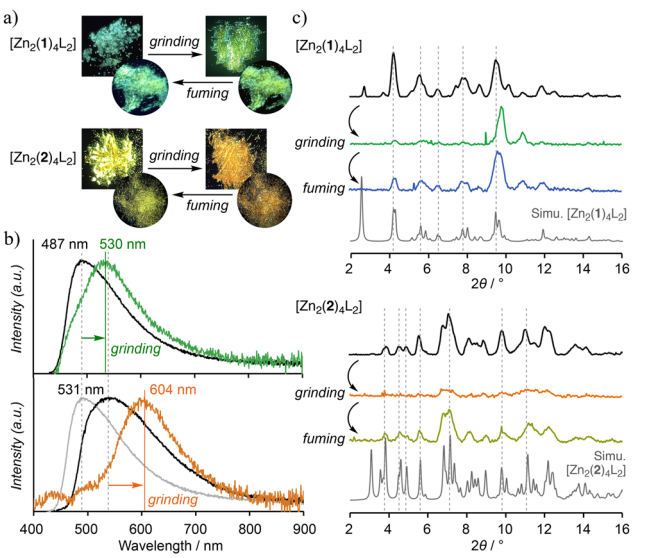

Fig. 5 (a) The appearance of before and after mechanical stimulation. (b) Normalized solid-state emission spectra: (top) before (black line) and after (green line) of $[Zn_2(\mathbf{1})_4L_2]$; (bottom) before (black line) and after (orange line) of $[Zn_2(\mathbf{2})_4L_2]$ with $[Zn_2(\mathbf{1})_4L_2]$ (gray line). (c) pXRD patterns of grinding and fuming of $[Zn_2(\mathbf{n})_4L_2]$ using MoK_α radiation.

These color changes were completely reversible; the original emission was restored within several minutes upon exposure to diethyl ether vapor. Powder X-ray diffraction (pXRD) patterns collected before and after grinding showed significant peak broadening, indicating partial amorphization, whereas vapor annealing recovered the sharp reflections of the initial crystalline phase (Fig. 5c). The close correlation between crystallinity and emission behavior confirms that the mechanochromic switching arises from reversible structural reorganization rather than chemical decomposition.

No remarkable mechanochromic response was observed for the free ligand L or the pyridine-capped $[Zn_2(\mathbf{n})_4Py_2]$, indicating that the adaptive nature of the $Zn_2(\mu\text{-carboxylate})_4$ core, coupled with the π-extended TPA–CC–Py ligand, is essential for the switching behavior. The larger red shift and enhanced Φ_{PL} after grinding in the fluorinated complex, $[Zn_2(\mathbf{2})_4L_2]$, can be attributed to its greater structural adaptability and the presence of π-hole⋯π interactions rather than conventional intermolecular interactions, which provide more directional and polarizable contacts under mechanical perturbation. In particular, fluorination increases the electrophilic character of the aromatic surfaces, which may enhance π-hole⋯π and related π⋯π interactions under compression, leading to stabilization of lower-energy excited states.

Hydrostatic-pressure dependence of photoluminescence

To obtain a more detailed understanding of the solid-state photoluminescence behavior of these complexes, high-pressure photoluminescence measurements were carried out (Fig. 6 and S21–25).[38–40] The measurements were performed using a diamond anvil cell, and the internal pressure was calibrated by the ruby fluorescence method. A single crystal used for the SC-XRD and variable-temperature experiments was employed as the sample. Perfluoropolyether (PFPE) oil was used as the pressure-transmitting medium.[41] Compression was applied from ambient pressure (0.0 GPa) to high pressure (3.5 or 3.6 GPa), and decompression was carried out from high pressure back to ambient pressure. During these processes, the emission spectra, crystal appearance, and emission colors were examined. Fig. 6a shows the photoluminescence spectra of the hydrogenated complex $[Zn_2(\mathbf{1})_4L_2]$ during compression and decompression. At ambient pressure, two emission maxima were observed at 467 nm and 492 nm (shoulder). Upon compression, both bands shifted slightly to longer wavelengths and retained similar spectral features up to 2.1 GPa, and an inversion of their relative intensities was observed. At higher pressures, the shorter wavelength emission disappeared, the emission maximum at 500 nm reached its highest intensity at 2.5 GPa, and a shoulder appeared at 530 nm. At 3.6 GPa, the averaged emission maximum was 525 nm, corresponding to a red-shift of approximately 60 nm (ΔE = 0.29 eV). The emission maximum shifted back to shorter wavelengths upon decompression, with largely retained spectral features. The spectral shapes were also similar during decompression. This reversibility was reflected in the crystal appearance, which changed from yellow brown to reddish brown, and in the emission color, which changed from blue (the hue angle, H = 175°) to green (H = 95°).

In comparison, the fluorinated complex $[Zn_2(\mathbf{2})_4L_2]$ showed smooth and pronounced red-shifts and larger emission color

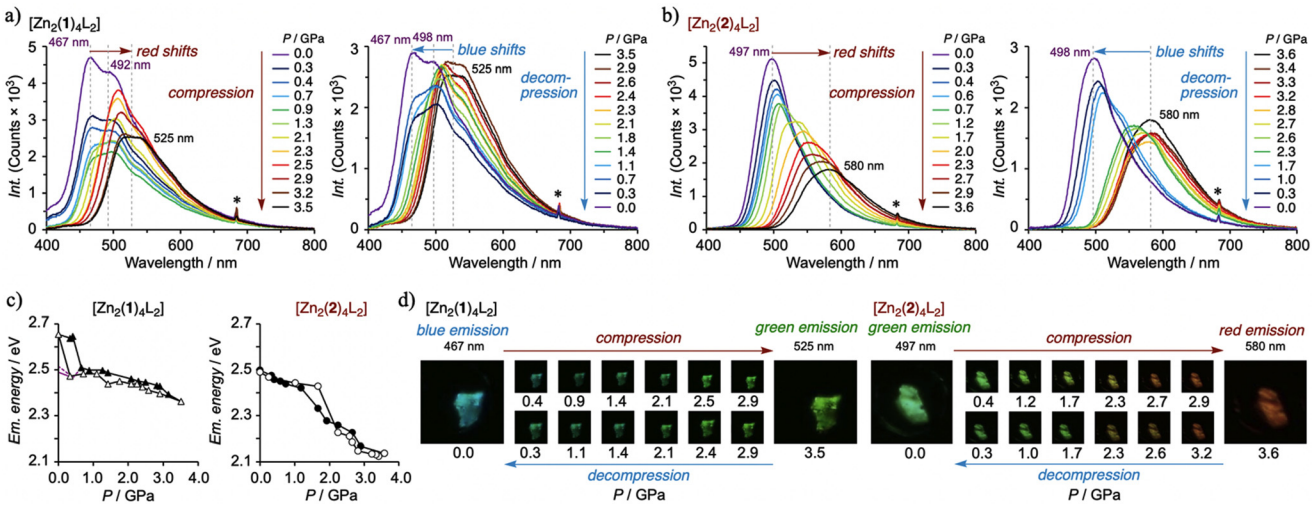

Fig. 6 Hydrostatic-pressure dependence of solid-state photoluminescence of single-crystals: photoluminescence spectra under compression (left) and decompression (right) of (a) $[Zn_2(\mathbf{1})_4L_2]$ and (b) $[Zn_2(\mathbf{2})_4L_2]$ under excitation at λ_{ex} = 365 nm (the asterisk represents the emission from the ruby); (c) plots of peak energies (peak maxima) *vs.* pressure for the complexes $[Zn_2(\mathbf{1})_4L_2]$ (left) and $[Zn_2(\mathbf{2})_4L_2]$ (right), with the part of color plots around 0.0–0.7 GPa in $[Zn_2(\mathbf{1})_4L_2]$ representing the average of two emission peaks; (d) photographic images of single crystals of $[Zn_2(\mathbf{1})_4L_2]$ (left) and $[Zn_2(\mathbf{2})_4L_2]$ (right) under hydrostatic pressure. The reversible cycle of multicolor emission (between green and red) is observed for $[Zn_2(\mathbf{2})_4L_2]$, whereas the color change of $[Zn_2(\mathbf{1})_4L_2]$ is tiny (between blue and green). The pressure for compression was increased from ambient pressure (0.0 GPa) to 3.5 or 3.6 GPa, and the corresponding decompression was performed in the reverse direction, from 3.5 or 3.6 GPa to ambient pressure (0.0 GPa).

changes during compression and decompression (Fig. 6b). At ambient pressure, the emission maximum was observed at 497 nm. During compression, this band shifted continuously to 580 nm at 3.6 GPa. The total shift was 83 nm (ΔE = 0.36 eV). Upon decompression, the emission maximum gradually returned to shorter wavelengths while maintaining similar spectral profiles. Although the crystal appearance changed from yellow brown to reddish brown in a manner similar to that of $[Zn_2(\mathbf{1})_4L_2]$, the emission colors were clearly different. The emission color changed from green (H = 135°) to yellow and then to orange red (H = 25°), indicating a distinct multicolor response. This pressure dependent luminescence behavior supports the qualitative trend observed in the mechanochromic response of $[Zn_2(\mathbf{2})_4L_2]$, which changes from yellowish green emission to orange emission. It also demonstrates that a single crystal provides a more uniform emission state than bulk samples. The continuous change in emission color during compression confirms that the fluorinated complex has a more flexible structure that can accommodate pressure more effectively than the hydrogenated analogue. While a single dominant interaction cannot be unambiguously identified, the consistent trends observed across the pressure range support this interpretation. Although the Zn_2 core itself is electronically silent and essentially colorless, paddlewheel type dinuclear Zn(II) complexes with conventional benzoate bridges usually exhibit blue emission in both solution and solid states, and the emission mainly originates from the ligand. When the bridging ligand was replaced with pentafluorobenzoate, the structural flexibility increased and the axial coordination interactions became stronger. As a result, the complex, $[Zn_2(\mathbf{2})_4L_2]$, showed multicolor emission ranging from blue to orange-red; blue (λ_{em} = 459 nm) in solution; green (497 nm) and greenish yellow (531 nm) in the solid state (single-crystal and precipitated microcrystalline state, respectively); orange (604 nm) and orange-red (580 nm) under mechanical and hydrostatic-pressure, while that of non-fluorinated $[Zn_2(\mathbf{1})_4L_2]$ showed blue to green colors (457–530 nm). Paddlewheel type Zn(II) dimers have been known for many years as interesting structural motifs. Fluorination enhances the axial coordination properties, enabling the emergence of new emission colors and pressure-responsive electronic states. The luminescence behavior of the Zn(II) complexes $[Zn_2(\mathbf{n})_4L_2]$ is not observed for the free ligand L or for the pyridine-capped analogues $[Zn_2(\mathbf{n})_4Py_2]$, and no new emission bands appear upon mechanical stimulation. In particular, for the fluorinated complex with ligand **2**, the emission shifts observed under mechanical grinding and hydrostatic pressure occur without the emergence of new peaks and are continuous in nature. These features do not suggest a discrete phase transition associated with a specific crystal system. Instead, the results are reasonably attributed to pressure-induced contraction of the zinc-bridged framework, which leads to effective extension of conjugation. This behavior demonstrates that the structural flexibility and external-field adaptability of the Zn_2(μ-carboxylate)$_4$ core, when combined with a π-electronic emissive ligand, play a central role in governing the luminescence response.

Experimental

General

All reagents and solvents were used without further purification. Compounds were characterized by EA, ^{1}H NMR, and crystallographic studies. ^{1}H NMR spectra were recorded on a JEOL AL400S spectrometer at 400 MHz using TMS as an internal standard. Electronic absorption spectra were measured on a JASCO V-660 UV/Vis spectrophotometer. Photoluminescence spectra and absolute quantum yields were obtained using a JASCO FP-8600 spectrometer and a Hamamatsu Photonics C9920-02G system, respectively. Solid-state temperature-dependent luminescence measurements were carried out using the single crystals. Samples were excited with a Panasonic Aicure UJ30 UV source through a UTVAF-34U UV-pass visible filter. Emission was collected through a 380 nm sharp-cut filter and focused into a Hamamatsu PMA-11 detector (model C7473) *via* a 1 mm quartz fiber. Temperature control was achieved using a LINKAM THMS 600 cooling–heating stage equipped with an LK-600PM controller and L-600A liquid-nitrogen cooling unit. Solid-state high-pressure luminescence measurements were performed using a diamond anvil cell. Pressures were calibrated by the ruby fluorescence method. Perfluoropolyether (PFPE) oil was used as the pressure-transmitting medium, and stainless-steel SUS301 gaskets (thickness 150 μm) with a 300 μm hole were used for sample loading.

Synthesis and physical properties

The π-extended ligand L was synthesized by a Sonogashira coupling between 4-bromopyridine and 4-ethynyl-*N*,*N*-diphenylaniline, as a reported procedure. The Zn(II) paddlewheel complexes $[Zn_2(\mathbf{n})_4L_2]$ and the pyridine analogues $[Zn_2(\mathbf{n})_4Py_2]$ (**n** = **1**, **2**) were prepared by reacting $Zn(OAc)_2{\cdot}2H_2O$ with the corresponding benzoic (**H1**) or pentafluorobenzoic acid (**H2**) in methanol in the presence of L or pyridine as axial donors. The products were isolated as microcrystalline solids and further purified by crystallization from $CHCl_3$ solution.

$[Zn_2(\mathbf{2})_4Py_2]$: colorless crystals (yield 52%). m.p. 121–122 °C. ^{1}H NMR ($CDCl_3$, TMS, ppm): δ 8.86 (d, J = 6.4 Hz, 4H, Py*H*); 8.01 (t, J = 6.4 Hz, 2H, Py*H*); 7.61 (t, J = 6.4 Hz, 2H, Py*H*). EA ($C_{38}H_{10}F_{20}N_2O_8Zn_2$): calcd C 40.28%, H 0.89%, N 2.47%; found C 40.02%, H 0.86%, N 2.45%.

$[Zn_2(\mathbf{1})_4L_2]$: yellow crystals (yield 80%). m.p. 210–212 °C. ^{1}H NMR ($CDCl_3$, TMS, ppm): δ 8.71 (d, J = 6.0 Hz, 4H, Py*H*); 8.13 (d, J = 8.0 Hz, 8H, Ph*H*); 7.53 (t, J = 8.0 Hz, 4H, Ph*H*); 7.48 (d, J = 6.0 Hz, 4H, Py*H*); 7.43–7.37 (m, 12H, Ph*H*); 7.29 (t, J = 8.0 Hz, 8H, Ph*H*); 7.13–7.07 (m, 12H, Ph*H*); 7.00 (d, J = 8.0 Hz, 4H, Ph*H*). EA ($C_{78}H_{56}N_4O_8Zn_2{\cdot}1.4CHCl_3$): calcd C 64.65%, H 3.92%, N 3.80%; found C 64.74%, H 3.52%, N 3.43%.

$[Zn_2(\mathbf{2})_4L_2]$: yellow crystals (yield 89%). m.p. 172–173 °C. ^{1}H NMR ($CDCl_3$, TMS, ppm): δ 8.73 (d, J = 6.0 Hz, 4H, Py*H*); 7.56 (d, J = 6.0 Hz, 4H, Py*H*); 7.38 (d, J = 8.0 Hz, 4H, Ph*H*); 7.29 (t, J = 8.0 Hz, 8H, Ph*H*); 7.13–7.09 (m, 12H, Ph*H*); 6.99 (d, J = 8.4 Hz, 4H, Ph*H*) ppm. EA ($C_{78}H_{36}F_{20}N_4O_8Zn_2$): calcd C 56.17%, H 2.18%, N 3.36%; found C 55.95%, H 2.21%, N 3.48%.

Conclusions

In summary, a new family of dumbbell-shaped Zn(II) paddlewheel dimers bearing π-extended TPA–CC–Py ligands was synthesized and fully characterized, showing a clear molecular framework for understanding how fluorination and axial coordination govern stimuli-responsive luminescence. The fluorinated complex displays enhanced structural flexibility, increased electronic anisotropy, and additional charge-transfer character, resulting in marked color modulation under mechanical grinding and hydrostatic pressure. These effects originate from cooperative changes in intermolecular contacts, π-hole-based interactions, and local packing distortions around the Zn_2(μ-carboxylate)$_4$ core. Both complexes show fully reversible mechanochromic switching, while only the fluorinated derivative exhibits continuous and large pressure-dependent color tuning across the visible range, from green to orange-red. The multicolor behavior in solution, crystalline solids, mechanically perturbed states, and under high pressure highlights the adaptability of the π-extended framework and underscores the importance of structural flexibility in controlling excited-state dynamics. These findings demonstrate that simple d^{10} paddlewheel architectures can be transformed into versatile and stimuli-responsive luminescent systems through judicious ligand design and fluorination. Although the Zn_2 core is electronically silent on its own, its combination with π-extended emissive ligands provides a structural linkage that enables broad color tunability and also governs, and in some cases enhances, the mechano- and pressure-responsive behavior of the chromophores. Owing to their reversible luminescence color changes in response to mechanical and hydrostatic stimuli, these Zn(II) paddlewheel complexes are promising candidates for pressure-responsive optical materials and mechanochromic luminescent sensors.

Author contributions

Y. T. performed synthesis of $[Zn_2(\mathbf{n})_4L_2]$ and crystallographic, spectroscopic, and theoretical studies, and wrote the draft. M. Y. synthesized $[Zn_2(\mathbf{n})_4Py_2]$ and crystallographic studies. I. T., Y. O., and M. A. performed the emission studies of thermal and hydrostatic-pressure dependence of single-crystals. A. H. supervised the project and wrote the manuscript. All authors contributed to discussions and to finalizing the manuscript.

Conflicts of interest

There are no conflicts to declare.

Data availability

The data supporting the findings of this study, including preparation methods, structural information, and physical properties, are available in the main article and its supplementary information (SI). Further inquiries regarding specific experimental details can be directed to the corresponding author. Additional information is available at the following sources:

Preparation of L: **https://doi.org/10.1016/j.dyepig.2017.07.043**

Preparation of complexes: **https://doi.org/10.1016/j.inoche.2006.07.013**

Supplementary information: NMR data; absorption and emission data; Hirshfeld analysis and DFT data. See DOI: **https://doi.org/10.1039/d5qi02451j**.

CCDC 2506028–2506031 contain the supplementary crystallographic data for this paper.[42a–d]

Acknowledgements

This work was supported by S-SPIRE project of Shibaura Institute of Technology (A. H.). M. A. acknowledges financial support from Special Research Projects Grant, University of Hyogo (FY2025). Y. O. acknowledges financial support for Grant-in-Aids for Scientific Research C, 22K05147, of JSPS KAKENHI.

References

1 F. Sánchez-Férez, R. Pou, L. Bayés-GarcÍa, M. Font-Bardia, J. Pons and J. A. Ayllón, Benzoate substituents effects on the structure of Zn(II) complexes and 1D 4,4′-bipyridine derived coordination polymers, *Inorg. Chim. Acta*, 2020, **500**, 119218, DOI: **10.1016/j.ica.2019.119218**.

2 C. Liu, J. Wang, L. Yan, Z. Chang, X. Bu, E. C. Sañudo and J. Ribas, Copper(II), Cobalt(II), and Nickel(II) Complexes with a Bulky Anthracene-Based Carboxylic Ligand: Syntheses, Crystal Structures, and Magnetic Properties, *Inorg. Chem.*, 2007, **46**, 6299–6310, DOI: **10.1021/ic070086y**.

3 E. V. Dikarev and B. Li, Rational Syntheses, Structure, and Properties of the First Bismuth(II) Carboxylate, *Inorg. Chem.*, 2004, **43**, 3461–3466, DOI: **10.1021/ic049937h**.

4 Y. Wang, H. Lin, W. Deng, C. Chen and L. Zhang, Tridentate Bromo-Substituted Porphyrin-Based Metal–Organic Framework Nanoflowers for Alkene Cyclopropanation, *ACS Appl. Nano Mater.*, 2025, **8**, 3175–3182, DOI: **10.1021/acsanm.4c07020**.

5 H. Inoue, Y. Yamashita, Y. Ozawa, T. Ono and M. Abe, Solid-State Structures and Photoluminescence of Lamellar Architectures of Cu(I) and Ag(I) Paddlewheel Clusters with Hydrogen-Bonded Polar Guests, *Molecules*, 2021, **26**, 6731–6745, DOI: **10.3390/molecules26216731**.

6 J. F. Berry, F. A. Cotton, S. A. Ibragimov, C. A. Murillo and X. Wang, Searching for Precursors to Metal–Metal Bonded Dipalladium Species: A Study of Pd_2^{4+} Complexes, *Inorg. Chem.*, 2005, **44**, 6129–6137, DOI: **10.1021/ic050876c**.

7 J. Wang, C. Liu, T. Hu, Z. Chang, C. Li, L. Yan, P. Chen, X. Bu, Q. Wu, L. Zhao, Z. Wang and X. Zhang, Zinc(II) coordination architectures with two bulky anthracene-

based carboxylic ligands: crystal structures and luminescent properties, *CrystEngComm*, 2008, **10**, 681–692, DOI: 10.1039/b710209g.

8 T. R. Cook, Y.-R. Zheng and P. J. Stang, Metal–Organic Frameworks and Self-Assembled Supramolecular Coordination Complexes: Comparing and Contrasting the Design, Synthesis, and Functionality of Metal–Organic Materials, *Chem. Rev.*, 2013, **113**, 734–777, DOI: 10.1021/cr3002824.

9 K. A. H. Alzahrani and R. J. Deeth, Molecular modeling of zinc paddlewheel molecular complexes and the pores of a flexible metal organic framework, *J. Mol. Model.*, 2016, **22**, 80, DOI: 10.1007/s00894-016-2949-5.

10 S. Perruchas, X. F. L. Goff, S. Maron, I. Maurin, F. Guillen, A. Garcia, T. Gacoin and J. Boilot, Mechanochromic and Thermochromic Luminescence of a Copper Iodide Cluster, *J. Am. Chem. Soc.*, 2010, **132**, 10967–10969, DOI: 10.1021/ja103431d.

11 M. G. Babashkina, D. A. Safin, M. Bolte and Y. Garcia, Mechanochromism of AgI complexes with *i*PrNHC(S)NHP(S)(O*i*Pr)$_2$, *Dalton Trans.*, 2011, **40**, 8523–8526, DOI: 10.1039/c1dt10688k.

12 A. Kobayashi and M. Kato, Stimuli-responsive Luminescent Copper(I) Complexes for Intelligent Emissive Devices, *Chem. Lett.*, 2017, **46**, 154–162, DOI: 10.1246/cl.160794.

13 D. Temerova, K. S. Kisel, T. Eskelinen, A. S. Melnikov, N. Kinnunen, P. Hirva, J. R. Shakirova, S. P. Tunik, E. V. Grachova and I. O. Koshevoy, Diversifying the luminescence of phenanthro-diimine ligands in zinc complexes, *Inorg. Chem. Front.*, 2021, **8**, 2549–2560, DOI: 10.1039/D1QI00149C.

14 S. D. Bella, Lewis acidic zinc(II) salen-type Schiff-base complexes: sensing properties and responsive nanostructures, *Dalton Trans.*, 2021, **50**, 6050–6063, DOI: 10.1039/D1DT00949D.

15 Y. Wada, T. Maruchi, R. Ishii and Y. Sunada, Visible Light Responsive Dinuclear Zinc Complex Consisting of Proximally Arranged Two d^{10}-Zinc Centers, *Angew. Chem., Int. Ed.*, 2023, **62**, e202310571, DOI: 10.1002/anie.202310571.

16 Z. Chi, X. Zhang, B. Xu, C. Ma, Y. Zhang, S. Liu and J. Xu, Recent advances in organic mechanofluorochromic materials, *Chem. Soc. Rev.*, 2012, **41**, 3878–3896, DOI: 10.1039/C2CS35016E.

17 X. Zhang, Z. Chi, Y. Zhang, S. Liu and J. Xu, Recent advances in mechanochromic luminescent metal complexes, *J. Mater. Chem. C*, 2013, **1**, 3376–3390, DOI: 10.1039/C3TC30316K.

18 E. Li, K. Jie, M. Liu, X. Sheng, W. Zhu and F. Huang, Vapochromic crystals: understanding vapochromism from the perspective of crystal engineering, *Chem. Soc. Rev.*, 2020, **49**, 1517–1544, DOI: 10.1039/C9CS00098D.

19 W. B. Jensen, The Place of Zinc, Cadmium, and Mercury in the Periodic Table, *J. Chem. Educ.*, 2003, **80**, 952, DOI: 10.1021/ed080p952.

20 F. Van Craeynest, W. Maenhout-Van Der Vorst and W. Dekeyser, Interpretation of the Yellow Colour of Heat Treated ZnO Powder, *Phys. Status Solidi*, 1965, **8**, 841–846, DOI: 10.1002/pssb.19650080322.

21 H. Chun, J. Kim, Y. Kim, M. J. Bae, M. M. Reddy and N. S. Dalal, Synthesis, X-ray Crystal Structures, and Gas Sorption Properties of Pillared Square Grid Nets Based on Paddle-Wheel Motifs: Implications for Hydrogen Storage in Porous Materials, *Chem. – Eur. J.*, 2005, **11**, 3521–3529, DOI: 10.1002/chem.200401201.

22 G. Mercuri, G. Giambastiani and A. Rossin, Thiazole- and Thiadiazole-Based Metal–Organic Frameworks and Coordination Polymers for Luminescent Applications, *Inorganics*, 2019, **7**, 144, DOI: 10.3390/inorganics7120144.

23 S. Mizukami, H. Houjou, K. Sugaya, E. Koyama, H. Tokuhisa, T. Sasaki and M. Kanesato, Fluorescence Color Modulation by Intramolecular and Intermolecular π–π Interactions in a Helical Zinc(II) Complex, *Chem. Mater.*, 2005, **17**, 50–56, DOI: 10.1021/cm049744s.

24 H. A. Habib, A. Hoffmann, H. A. Höppe, G. Steinfeld and C. Janiak, Crystal Structure Solid-State Cross Polarization Magic Angle Spinning ^{13}C NMR Correlation in Luminescent d^{10} Metal-Organic Frameworks Constructed with the 1,2-Bis(1,2,4-triazol-4-yl)ethane Ligand, *Inorg. Chem.*, 2009, **48**, 2166–2180, DOI: 10.1021/ic802069k.

25 T. Ohmura, W. Mori, T. Takei, T. Ikeda and A. Maeda, Structure and magnetic behaviour of mononuclear and dinuclear Cu(II)/Zn(II) monocarboxylate-pyridine derivatives studied by crystal engineering, *Mater. Sci.*, 2005, **23**, 729–736.

26 A. Karmakar, R. J. Sarma and J. B. Baruah, Self-assembly of neutral dinuclear and trinuclear zinc-benzoate complexes, *Inorg. Chem. Commun.*, 2006, **9**, 1169–1172, DOI: 10.1016/j.inoche.2006.07.013.

27 Q. Zhou, T. W. Hambley, B. J. Kennedy, P. A. Lay, P. Turner, B. Warwick, J. R. Biffin and H. L. Regtop, Syntheses and Characterization of Anti-inflammatory Dinuclear and Mononuclear Zinc Indomethacin Complexes. Crystal Structures of $[Zn_2(Indomethacin)_4(L)_2]$ (L = *N,N*-Dimethylacetamide, Pyridine, 1-Methyl-2-pyrrolidinone) and $[Zn(Indomethacin)_2(L_1)_2]$ (L_1 = Ethanol, Methanol), *Inorg. Chem.*, 2000, **39**, 3742–3748, DOI: 10.1021/ic991477i.

28 D. L. Reger, A. Debreczeni and M. D. Smith, Zinc Paddlewheel Dimers Containing a Strong π···π Stacking Supramolecular Synthon: Designed Single-Crystal to Single-Crystal Phase Changes and Gas/Solid Guest Exchange, *Inorg. Chem.*, 2011, **50**, 11754–11764, DOI: 10.1021/ic201830h.

29 A. M. Baruah, A. Karmakar and J. B. Baruah, Steric effects in controlling co-ordination environment in zinc 2-nitrobenzoate complexes, *Inorg. Chim. Acta*, 2008, **361**, 2777–2784, DOI: 10.1016/j.ica.2008.01.044.

30 K. F. Konidaris, M. Kaplanis, C. P. Raptopoulou, S. P. Perlepes, E. Manessi-Zoupa and E. Katsoulakou, Dinuclear versus trinuclear complex formation in zinc(II) benzoate/pyridyl oxime chemistry depending on the position of the oxime group, *Polyhedron*, 2009, **28**, 3243–3250, DOI: 10.1016/j.poly.2009.05.076.

31 W. Wang, W. X. Wu, Y. Zhang and W. J. Jin, Perfluoroaryl···aryl interaction: The most important subset of π-hole···π bonding, *Chem. Phys. Rev.*, 2024, **5**, 031303, DOI: 10.1063/5.0205540.

32 Y. Ikumura, T. Kawasaki, Y. Ishida, H. Usui, S. Uchida, K. Kamata, M. Nomura and A. Hori, Boosting CO_2 and benzene adsorption through π-hole substitution in β-diketonate Cu(II) complex within non-porous adaptive crystals, *RSC Adv.*, 2025, **15**, 6184–6190, DOI: 10.1039/d4ra08463b; K. Nakada, G. J. Richards and A. Hori, Colorimetric Detection of Naphthalene Enabled by Intra- to Intermolecular Charge Transfer Interplay Induced by π-hole···π Interactions of a TPA-Attached Pyrazinacene, *Chem. – Eur. J.*, 2025, **31**, e202404487, DOI: 10.1002/chem.202404487.

33 J. Tydlitát, S. Achelle, J. RodrÍguez-López, O. Pytela, T. Mikýsek, N. Cabon, F. R. Guen, D. MiklÍk, Z. Ruzickova and F. Bures, Photophysical properties of acid-responsive triphenylamine derivatives bearing pyridine fragments: Towards white light emission, *Dyes Pigm.*, 2017, **146**, 467–478, DOI: 10.1016/j.dyepig.2017.07.043.

34 M. A. Spackman and D. Jayatilaka, Hirshfeld surface analysis, *CrystEngComm*, 2009, **11**, 19–32, DOI: 10.1039/B818330A.

35 M. J. Turner, J. J. McKinnon, S. K. Wolff, D. J. Grimwood, P. R. Spackman, D. Jayatilaka and M. A. Spackman, *CrystalExplorer 17*, 2017.

36 T. Saito, M. Yoshida, K. Segawa, D. Saito, J. Takayama, S. Hiura, A. Murayama, N. M. Lakshan, W. M. C. Sameera, A. Kobayashi and M. Kato, Thermo-responsive emission induced by different delocalized excited-states in isomorphous Pd(ii) and Pt(II) one-dimensional chains, *Chem. Sci.*, 2024, **15**, 14497–14505, DOI: 10.1039/D4SC04497E.

37 H. Kitagawa, Y. Ozawa and K. Toriumi, Flexibility of cubane-like Cu_4I_4 framework: temperature dependence of molecular structure and luminescence thermochromism of $[Cu_4I_4(PPh_3)_4]$ in two polymorphic crystalline states, *Chem. Commun.*, 2010, **46**, 6302–6304, DOI: 10.1039/C0CC01434F.

38 T. Ono, Y. Tsukiyama, A. Taema, H. Sato, H. Kiyooka, Y. Yamaguchi, A. Nagahashi, M. Nishiyama, Y. Akahama, Y. Ozawa, M. Abe and Y. Hisaeda, Piezofluorochromism in Charge-Transfer Inclusion Crystals: The Influence of High Pressure versus Mechanical Grinding, *ChemPhotoChem*, 2018, **2**, 416–420, DOI: 10.1002/cptc.201700227.

39 H. Liu, Y. Gu, Y. Dai, K. Wang, S. Zhang, G. Chen, B. Zou and B. Yang, Pressure-Induced Blue-Shifted and Enhanced Emission: A Cooperative Effect between Aggregation-Induced Emission and Energy-Transfer Suppression, *J. Am. Chem. Soc.*, 2020, **142**, 1153–1158, DOI: 10.1021/jacs.9b11080.

40 A. N. Sussardi, G. F. Turner, J. G. Richardson, M. A. Spackman, A. T. Turley, P. R. McGonigal, A. C. Jones and S. A. Moggach, Tandem High-Pressure Crystallography–Optical Spectroscopy Unpacks Noncovalent Interactions of Piezochromic Fluorescent Molecular Rotors, *J. Am. Chem. Soc.*, 2023, **145**, 19780–19789, DOI: 10.1021/jacs.3c05444.

41 S. Irii, T. Ogaki, S. Yamamoto, H. Miyashita, K. Nobori, H. Iida, Y. Ozawa, M. Abe, H. Sato, Y. Matsui and H. Ikeda, The role of a [2.2]paracyclophane moiety in piezofluorochromism of crystalline organoboron complexes, *J. Mater. Chem. C*, 2026, **14**, 232–242, DOI: 10.1039/D5TC03195H.

42 (*a*) CCDC 2506028: Experimental Crystal Structure Determination, 2026, DOI: 10.5517/ccdc.csd.cc2q3qm6; (*b*) CCDC 2506029: Experimental Crystal Structure Determination, 2026, DOI: 10.5517/ccdc.csd.cc2q3qn7; (*c*) CCDC 2506030: Experimental Crystal Structure Determination, 2026, DOI: 10.5517/ccdc.csd.cc2q3qp8; (*d*) CCDC 2506031: Experimental Crystal Structure Determination, 2026, DOI: 10.5517/ccdc.csd.cc2q3qq9.